Eur. Phys. J. B **17**, 603–608 (2000)

THE EUROPEAN PHYSICAL JOURNAL B

EDP Sciences

Photoemission study of the carrier bands in Bi(111)

M. Hengsberger[a,b], P. Segovia, M. Garnier[c], D. Purdie, and Y. Baer

Institut de Physique, Université de Neuchâtel, 1 rue A.-L. Breguet, 2000 Neuchâtel, Switzerland

Received 8 June 2000

Abstract. We present high-resolution photoemission data from the Bi(111)-surface. The electronic structure of the semimetal close to the Fermi level has been found to change dramatically with respect to the well established bulk band structure. The Fermi surfaces observed for the electron and hole bands resemble those of the next group-V element, antimony, probably as a consequence of surface relaxation. This results in a relatively high surface charge density. The observed temperature dependence of the electron Fermi energy confirms this result.

PACS. 79.60.-i Photoemission and photoelectron spectra – 73.20.At Surface states, band structure, electron density of states

1 Introduction

Bismuth is the last of a series of semimetals in the group V of the periodic table of elements. Its bulk properties have been widely studied in the last decades and have led to the discovery of important experimental methods (for a review, the reader is referred to the article of Édel'man [1]). Calculations of the electronic band structure of bulk Bi demand very refined numerical models, including relativistic effects owing to the heavy atomic mass and to the small energy scales involved [2–5]. Bi crystallizes in the rhombohedral A7-structure emerging from the simple cubic lattice by two independent distortions: an internal displacement of the two intercalating fcc-sublattices and a shear along the trigonal [111]-direction [4,6]. In hexagonal coordinates, the lattice can be represented as a stack of layers along [111], each layer comprising two hexagonal planes [7]. The slight lattice distortion in line with a strong spin-orbit-coupling causes a small overlap of two bands around the Fermi energy, resulting in an almost filled band with small negative effective mass, *i.e.* the *hole* band, and an almost empty *electron* band. The carrier density of about 3×10^{17} electrons or holes per cm^3 [8] is comparable to that of a fairly doped semiconductor. The Brillouin zone (BZ) is almost identical to that of a fcc-structure except for the hexagonal (111) zone faces which are inequivalent to those of the {[100]}-directions. The corresponding symmetry points in the center of these faces, commonly named T and L, respectively, are the centers of the hole and electron Fermi surfaces [2–5] (see Fig. 1).

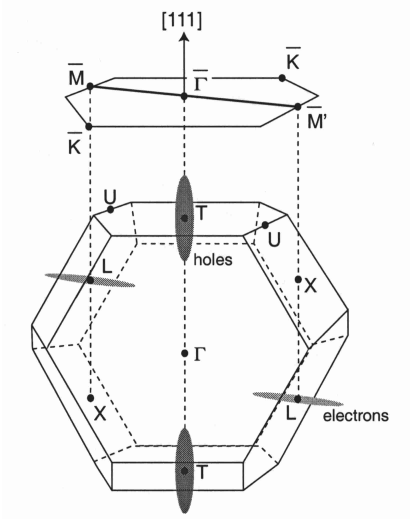

Fig. 1. Brillouin zone of the rhombohedral lattice. At the top, the SBZ is shown for the (111)-surface. The projection of the ΓTULX-mirror plane of the bulk onto the (111)-face yields the $\overline{\mathrm{M}'\Gamma\mathrm{M}}$-line of the SBZ. The position and topology of the bulk Fermi surfaces are indicated by the grey shaded ellipsoids (size not to scale).

Bi has achieved renewed interest in the last years due to its peculiar band structure which makes it a suitable candidate for experiments on a nanometer scale: in an isotropic electron gas, the same carrier density along with a Fermi energy of 23–27 meV [8,9] yields the following properties: parabolic dispersion with an effective mass of 0.06 times the electron rest mass m_0, a Fermi wavelength,

[a] e-mail: matthias@physik.unizh.ch
[b] *New address:* Physikinstitut, Universität Zürich-Irchel, Winterthurerstr. 190, 8057 Zürich, Switzerland
[c] *Present address:* Institut für Physik, Universität Basel, Klingelbergstr. 82, 4056 Basel, Switzerland

important for quantum size experiments, of the order of 100 Å, and a Thomas-Fermi-screening length of roughly 30 Å. These length scales render the observation of quantum size effects [10–14] or the formation of interfaces in heterostructures [15–18] in large geometries possible. The (111)-surface is particularly important, since the growth of Bi films on substrates like mica or GaAs stabilizes for large thicknesses in this orientation [10,19]. This surface does not reconstruct and is chemically inert, and its electronic structure is generally believed to be representative of the bulk. This is a crucial point if experiments are carried out using surface sensitive methods as photoemission (PE) and electron-energy-loss spectroscopy. The damping of quantum oscillations with decreasing film thickness in thin films [20] and the occurrence of superconductivity in granular systems with high surface/volume-ratio [21] suggest indeed changes in the electronic structure due to the bulk termination. Several photoemission studies established the presence of strong surface states and resonances [22–25] and a large surface core level shift [23]. The most intriguing result, however, is the appearance of a strong Fermi edge in normal emission spectra, contrasting with the expected low density of states of this material [23]. Aim of the present work was therefore to verify, whether the bulk carrier bands can be observed in PE spectra, and to look for differences between the bulk and the surface electronic structure.

In this work we present the first photoemission study of the bands close the Fermi energy of Bi, which are relevant for the thermodynamic properties. It is anticipated that the observation of the carrier bands sets stringent constraints for the photoemission experiment. At 48 K [26], the Debye temperature of the Bi(111)-surface is very low, and cooling to liquid He temperature is therefore indispensable if phonon-assisted indirect transitions are to be minimized [27]. The typical band width of the carrier bands is of the order of room temperature, *i.e.* 25 meV, and some effective band masses are of the order of $0.05m_0$. A reasonable signal intensity can only be achieved if the angular resolution is lowered, and, as a consequence, the corresponding resolution in k-space is not sufficient to resolve the dispersion in directions of small effective mass.

This paper is organized as follows: in Section 2, the experimental apparatus and the sample preparation are described, in Section 3 we will present the photoemission results, followed by the conclusion in Section 4.

2 Experiment

The sample was mechanically polished prior to insertion into vacuum and cleaned *in situ* by cycles of sputtering (1 keV Ar ions) and annealing (160 °C). Cleanliness was checked with Auger electron spectroscopy and X-ray photoemission spectroscopy. The surface order was verified by low-energy-electron diffraction (LEED) and exhibited a sharp trigonal pattern [28].

The spectrometer is equipped with a hemispherical electron analyser and two He discharge lamps, the angle between the incident light and the detector being fixed to $\pm 45°$. Spectra at different emission angles are taken by rotation of the sample in the plane spanned by the electron analyzer and the incident light beams. A quartz capillary serves as light guide for one of the photon sources. Use of a double-focusing monochromator with the second source to separate out the various excitation lines has the additional effect of producing highly linearly polarised light (about 90%). The monochromator unit can be rotated in order to place the polarisation vector either in, or perpendicular to, the measurement plane, respectively referred to hereafter as p- and s-polarisation. All spectra presented here have been taken with HeI-photons (21.2 eV). The two-dimensional detector of our spectrometer allows furthermore the angular distribution of the photoemitted electrons to be recorded within about $\pm 5°$ *perpendicular* to the measurement plane. The energy and angular resolutions of our spectrometer were set to 5 meV and $\pm 0.5°$, respectively. The corresponding resolution in reciprocal space is better than 0.037 $Å^{-1}$. The sample can be cooled down to 12 K by use of a He flow cryostat.

3 Results and discussion

The Brillouin zone (BZ) of the A7-lattice is shown in Figure 1 together with a sketch of the bulk Fermi surfaces. The (111)-surface BZ (SBZ) has been added. The symmetry points are labeled according to the commonly used notation [2]. The plane of interest is the mirror plane σ or ΓTULX (Fig. 1), whose projection of the (111)-surface corresponds to the $\overline{\mathrm{M}'\Gamma\mathrm{M}}$-line. The latter is emphasized in Figure 1.

The bulk Fermi surface of Bi consists of electron pockets centered at the six L-points of the bulk BZ and hole pockets at the T-points (see Fig. 1). Projected onto the (111)-surface under investigation here, one expects therefore to observe a band with very small negative effective mass crossing the Fermi level twice symmetrically around normal emission and a free-electron like band, centered at $\overline{\mathrm{M}}$, along the $\overline{\Gamma\mathrm{M}}$-direction of the surface BZ, *i.e.* the hole and the electron bands, respectively. Spectra, taken with p-polarised HeI-photons at these symmetry points, are displayed in Figure 2. The inequivalence of the two directions $\overline{\Gamma\mathrm{M}}$ and $\overline{\Gamma\mathrm{M}'}$ is unambiguously reflected in the spectra. We want to focus our attention on the features highlighted by arrows in Figure 2 and refer to the strong peak seen in normal emission as the hole band, to the weak structure at $\overline{\mathrm{M}}$ as the electron band. As can be seen in the inset, this latter peak is observed in both directions. Because of the small signal intensity in the spectrum taken at $\overline{\mathrm{M}'}$, we restrict the analysis to the $\overline{\mathrm{M}}$-point.

Furthermore, the peak observed at about 1.2 eV binding energy in normal emission can be used to locate the probed wavevector in the three-dimensional BZ: the extrema of this band correspond to initial state energies of about 0.8 eV at Γ and 1.4 eV at T [7]. A simple comparison yields a wavevector in the vicinity of the T-point for normal emission and HeI-photons.

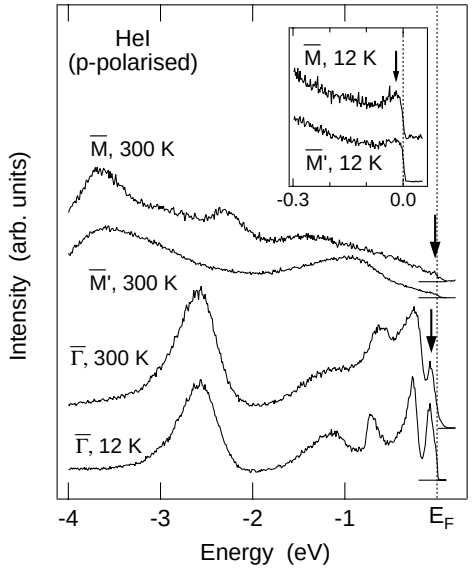

Fig. 2. Valence band spectra, taken with p-polarised HeI photons at various symmetry points. Arrows indicate the features of interest. The inset shows a zoom onto the Fermi level at the border of the SBZ, where the electron bands are observed.

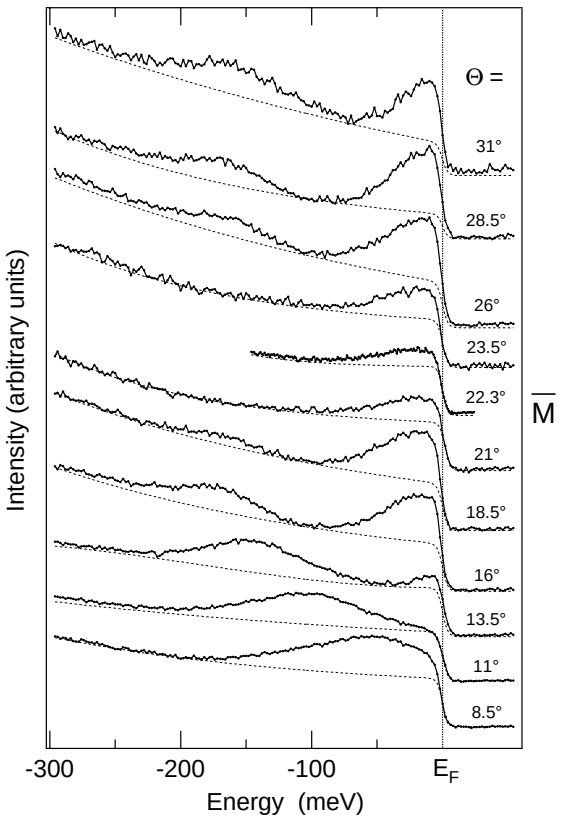

Fig. 3. Series of selected spectra around the $\overline{\mathrm{M}}$ symmetry point, taken with unpolarised HeI photons at 12 K in the $\Gamma TULX$ bulk mirror plane. Θ gives the emission angle with respect to the surface normal. The dashed lines underneath the spectra denote featureless background.

3.1 Electrons

The spectra displayed in Figure 3 show the appearance of a peak at about 13.5° dispersing slowly towards the point of maximum binding energy at 22.3°. This angle corresponds to the border of the SBZ or the projection of the L-point of the bulk BZ onto the (111)-surface. At higher angles, a slow upward dispersion is observed. The spectra have been taken with the unmonochromatised lamp. Using the monochromatised source, the peaks appear only if excited with p-polarised light. The initial state belongs, therefore, to a wavefunction with even symmetry under reflection at the mirror plane. In accord with band structure calculations it can be attributed to the electron band with even L_4-symmetry at the border of the BZ [2,29]. A second band is observed at slightly higher binding energy. Its dispersion is roughly parallel to that of the electron band. No evidence of a band with expected mirror-like dispersion [2,9] was found around the $\overline{\mathrm{M}}$ point. The next observation is the peak intensity which diminishes at the $\overline{\mathrm{M}}$ symmetry point. The second band observed in the spectra even vanishes at this angle indicating that a gap in the final state bands probably opens up at the zone boundary corresponding to $\overline{\mathrm{M}}$. Attempts were made to measure the dispersion perpendicular to the symmetry plane by direct imaging of the second detector dimension, but the strong dispersion could not be resolved in angle.

Thus, at a first glance, the measured electron band resembles to what is expected from band structure calculations and measurements of the bulk Fermi surface. Centered at the border of the SBZ, it disperses in a quasi-parabolic manner towards the Fermi energy with the heavy mass direction along the bisectrix in the mirror plane (Fig. 4). The transversal effective mass, *i.e.* along the binary axis of the crystal lattice, is several orders of magnitude smaller. The bulk value of the heavy mass being of the order of the free electron rest mass [1], a comparison with our data however shows that the observed heavy mass must be much larger. As visualized in Figure 4, this effective mass can roughly be estimated to yield $7.5m_0$. Furthermore, spectra taken at 300 K (not shown here) reveal that the Fermi wave vector does only slightly depend on temperature over the whole temperature range. Thus, the heavy effective mass seems to be independent of temperature.

3.2 Temperature dependence

Additional information about the dispersion of the electron band can be obtained from the temperature dependence of the occupied width of the electron band [30]. The change of the band width with temperature gives some rough indication of the energy gap between the two bands at the L-point ($\overline{\mathrm{M}}$) and the effective mass tensor [9]. In our experiment, the electron band width is measured as the initial state energy relative to E_F at the $\overline{\mathrm{M}}$-point.

Photoemission data, which have been recorded at 12, 60 and 300 K, are displayed in Figure 5. The background, as extrapolated from valence band spectra at higher binding energies, is indicated as dashed line.

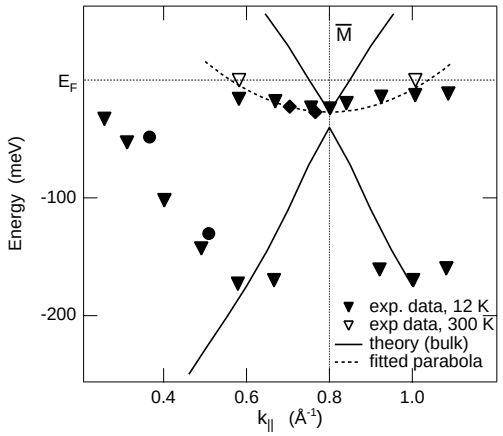

Fig. 4. Plot of the peak maxima *vs.* wave vector $k_{\|}$ along $\overline{\Gamma\mathrm{M}}$: Open triangles denote the Fermi momentum at 300 K, solid symbols peak maxima at 12 K (triangles, diamonds, circles for data obtained using unpolarised, *s*-polarised, and *p*-polarised light, respectively). The bulk dispersion, calculated using a tight-binding scheme [5], is indicated by the thick lines. The dashed line corresponds to parabolic dispersion with an effective mass of $7.5m_0$.

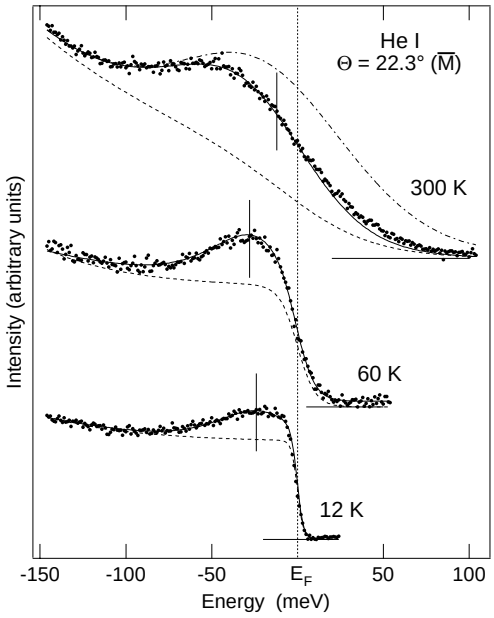

Fig. 5. Spectra at the $\overline{\mathrm{M}}$-point (dots), taken with unpolarised HeI-photons at different temperatures. Dashed lines show the background, as extrapolated from the valence band spectra at higher binding energy. The fits (solid lines) are described in detail in the text, the vertical lines denote the corresponding initial state energies. The dashed-dotted line in the 300 K-spectrum is the Gaussian shape resulting from the fit prior to multiplication with the Fermi function.

For the low temperature spectra, the peak shapes were then fitted with Lorentzians, multiplied with the Fermi function. The values found were 24 ± 3 meV at 12 K and 28 ± 3 meV at 60 K, in excellent agreement with those reported for bulk Bi (≈ 27 meV for $T \leq 80$ K [9]). In the high temperature spectrum, however, the strong background and the thermal broadening render a reliable fitting almost impossible. The most successful, but nevertheless ambiguous, way to find the peak position has been to divide the spectrum by the Fermi function and to fit the result by a Gaussian. In this way, a value of 12 ± 2 meV is found, thus a slight reduction of the occupied band width with increasing temperature. Heremans and Hansen have computed the bulk electron Fermi energy assuming different temperature dependencies of the effective mass tensor [9]. A value of 12 meV at 300 K would be in accord with the calculation, if the *heavy* mass were temperature-independent, thus in agreement with our experimental findings described in the preceding section. However, in order to reconcile thermopower data and bulk band structure calculations at high temperature, a fully temperature-dependent effective mass tensor and contributions from the thermally depopulated second band at the L-point have to be assumed at high temperature [9]. This results in an increase of the electron Fermi energy with increasing temperature, in contradiction to our results. Hence, the temperature dependence of the electron band width together with the observed large effective mass give clear evidence that the dispersion of the electron band is strongly altered at the sample surface.

3.3 Holes

The band structure near E_{F} around normal emission is quite complex and contains several features. The most contrasted spectra can be obtained by use of *s*-polarised light. Some selected curves are displayed in Figure 6a. They have been taken at 12 K and are normalized to the measurement time. They show a peak at normal emission moving towards the Fermi level with increasing negative angle (direction $\overline{\Gamma\mathrm{M}}'$), crossing E_{F} at about $-4°$ off-normal and moving back at about $-8°$. For positive angles, a similar behaviour is observed, but with less intensity. The same observations hold for *p*-polarised light (not shown here), but the structures are smeared out due to the presence of a strong second peak dispersing in the opposite direction. The initial state contains therefore symmetric and antisymmetric contributions with regard to the mirror plane, as it should be for the bulk hole band (symmetry label λ_{45} [2]).

A more figurative view is obtained if the spectra are displayed as greyscale plot with the abscissa and ordinate corresponding to the emission angle and binding energy, respectively. This is shown in Figure 6 for *p*-polarised (b) and *s*-polarised (c) light. Some of the spectra have been interpolated in order to get a continuous picture. The calculated dispersion of the bulk hole band has been added for comparison. The intensity seen around normal emission at energies below -200 meV stems from the surface state in the spin-orbit gap [22]. It is obvious that the hole band at the Fermi level is centered *off* normal emission for negative angles. The same holds for the opposite direction $\overline{\Gamma\mathrm{M}}$, whereas no indication for a bulk-like hole band is found. The observed band has a negative effective mass

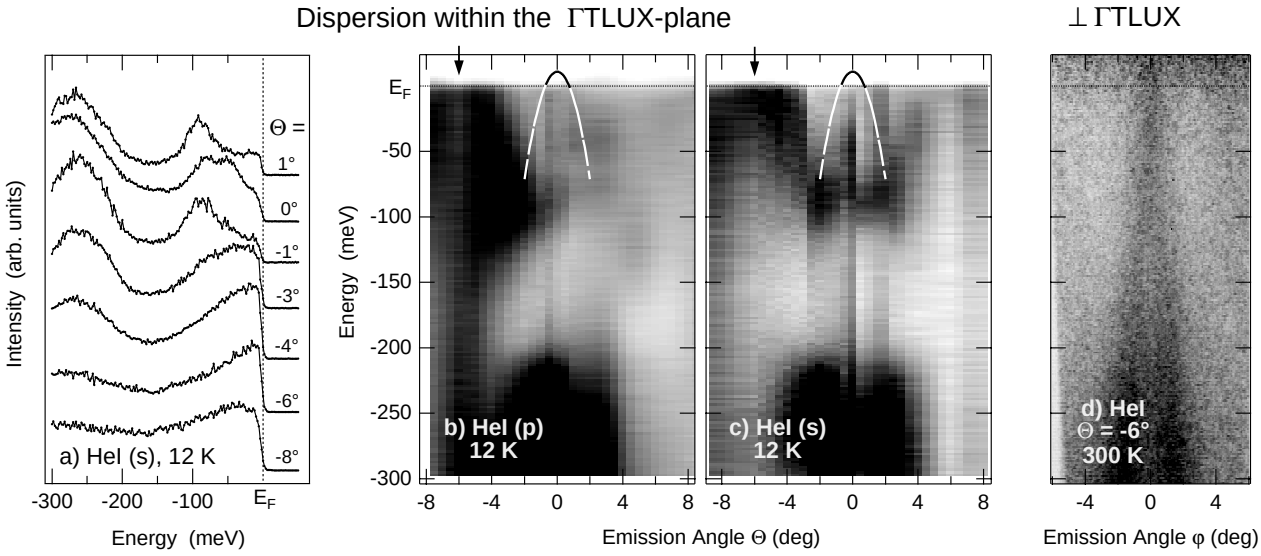

Fig. 6. (a) Spectra, taken around normal emission with *s*-polarised HeI-photons at 12 K; spectra are normalized to the measurement time. (b) and (c) Greyscale plot of spectra (HeI, 12 K), taken around normal emission along $\overline{\Gamma\mathrm{M}}$ using *p*-polarised (b) and *s*-polarised (c) light; black = high intensity; arrows indicate where the picture (d) has been taken. The solid line denotes the expected dispersion of the bulk hole band. (d) Direct image of the detector, displayed for an emission angle $\Theta = -6°$. It represents the dispersion of the band *perpendicular* to the actual measurement plane (unpolarised light, 300 K).

as shown in Figure 6d by a direct image of our detector in the direction perpendicular to the symmetry plane (emission angle $\Theta = -6°$, indicated by arrows in parts (b) and (c)). The image was taken at 300 K and reported on a logarithmic intensity scale in order to follow the dispersion as far as possible beyond the Fermi energy. In a parabolic approximation, *i.e.*

$$E(k) = \frac{\hbar^2 k^2}{2m^\star} + E_0,$$

the dispersion corresponds to an effective mass of about $m^\star \approx -0.04\, m_0$ and $E_0 - E_\mathrm{F} \approx 15$ meV. The hole band can be observed over an energy range of about 170 meV between $\overline{\Gamma}$ and the $\overline{\mathrm{M}}$-point, yielding roughly 185 meV of total band width. This, compared to about 2.6 eV for the bulk band [5], gives further evidence for surface character of the carrier bands.

Finally, in order to establish the symmetry of the found Fermi surface and to exclude a possible sample misalignment, a Fermi surface mapping was carried out (Fig. 7). It was recorded with *s*-polarised HeI-radiation at 12 K, integrating over an energy window of 20 meV centered at the Fermi energy. It shows three intense pockets elongated within the mirror planes in $\overline{\Gamma\mathrm{M}}'$-direction and an analogue set related by inversion at the $\overline{\Gamma}$-point with weaker intensity. The surface has *a priori* no inversion symmetry, nor exists a reciprocal lattice vector to relate the two sets *via umklapp* scattering. The presence of the second set indicates that contributions of at least the two bilayers are observed since one bilayer possesses trigonal symmetry [7]. This explains at the same time the difference in intensity between both sets.

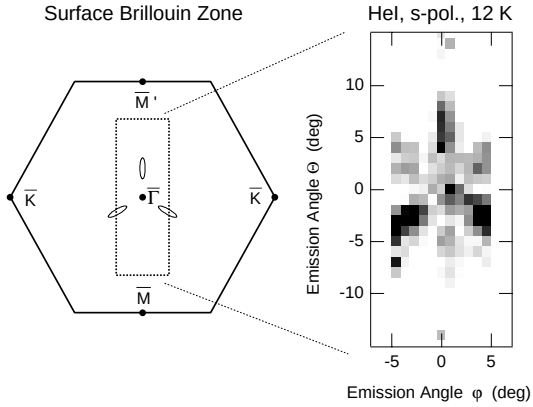

Fig. 7. Fermi surface mapping of the hole surfaces. The photoemission intensity (right panel) at E_F (energy window ± 10 meV, *s*-polarised HeI photons, 12 K; black = high intensity) was probed as function of emission angle, corresponding to momenta within the dashed rectangle on the left-hand-side. Three pockets with high intensity and a similar set, rotated by 180° around the trigonal axis, are observed.

4 Conclusion

Summarizing our results we can propose a band structure for the Bi(111)-surface, which is displayed in Figure 8 beside the projection of the bulk band structure. Effective mass and Fermi wave vector of the electrons are much larger than the corresponding bulk values. Although no information is available on the third dimension of the Fermi surface, the suggestion of a much higher carrier density for the surface seems to be reasonable.

The measured Fermi surfaces are very similar to the Fermi surfaces of bulk Sb, *i.e.* six hole pockets

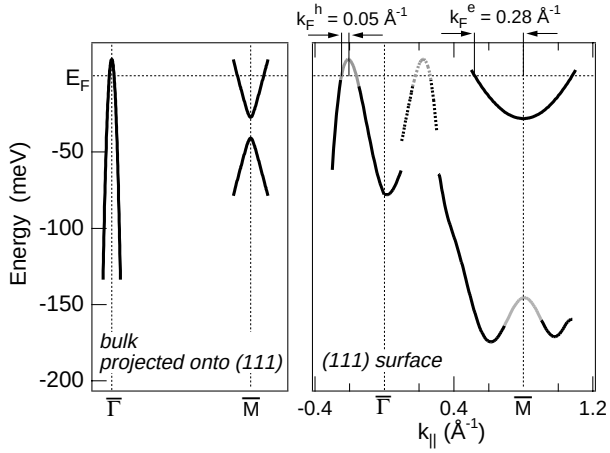

Fig. 8. Comparison of the bulk band structure of Bi [5], projected onto the (111)-surface (on the left-hand-side), and the proposed surface band structure (on the right-hand-side). The grey parts of the bands are a reasonable continuation of our data; the dashed line denotes the dispersion of a weak feature in the spectra and is likely to be related to contributions from the adjacent bilayer.

in the reflection planes and large electron pockets around the L-points of the bulk BZ [29,31]. The only difference between the Sb and the Bi crystal lattice apart from the inter-atomic distances is the deviation from the cubic structure, larger by roughly 4% for Sb than for Bi. Supposed that the topmost layer of the Bi surface differs somewhat from its *ideal* structure by a slight relaxation of the surface atoms, the surface electronic structure of Bi could become to a certain extent "antimony-like". Since the carrier density in bulk Sb is roughly two orders of magnitude higher than that of bulk Bi, our results could explain the high density of states on the Bi surface [23]. This is partially confirmed by calculations of the surface electronic structure using the Green's function transfer method [32]. The authors conclude that bona fide surface states can be obtained in calculations only if the surface atoms are allowed to relax.

In conclusion, we presented the first photoemission study of the carrier bands in Bi(111). This study confirms that the electronic structure of Bi close to the Fermi energy depends very critically on lattice parameters. It is therefore not quite surprising to observe that UV-photoemission spectra of Bi(111) do not probe the carrier bands of the bulk which offer exceptional conditions for testing quantum size effects. Our assumption of an "antimony-like" character of the Bi states in the surface region provides a quite natural explanation of our data but needs to be confirmed by an experimental determination of the surface relaxation and a surface band structure calculation including the local deviation from the bulk parameters.

We are indebted to W.-D. Schneider for the loan of the Bismuth single crystal. This work was funded by the Fonds National Suisse de la Recherche Scientifique.

References

1. V.S. Édel'man, Adv. Phys. **25**, 555 (1976).
2. S. Golin, Phys. Rev. **166**, 643 (1968).
3. J. Rose, R. Schuchardt, Phys. Status Solidi B **117**, 213 (1983).
4. X. Gonze, J.-P. Michenaud, J.-P. Vigneron, Phys. Rev. B **41**, 11827 (1990).
5. Y. Liu, R.E. Allen, Phys. Rev. B **52**, 1566 (1995).
6. R.J. Needs, R.M. Martin, O.H. Nielsen, Phys. Rev. B **33**, 3778 (1986).
7. G. Jezequel, J. Thomas, I. Pollini, Phys. Rev. B **56**, 6620 (1997).
8. R.J. Dinger, A.W. Lawson, Phys. Rev. B **7**, 5215 (1973).
9. J. Heremans, O.P. Hansen, J. Phys. C **12**, 3483 (1979).
10. N. Garcia, Y.H. Kao, M. Strongin, Phys. Rev. B **5**, 2029 (1972).
11. V. de Renzi, M.G. Betti, C. Mariani, Phys. Rev. B **48**, 4767 (1993).
12. J.L. Costa-Krämer, N. García, H. Olin, Phys. Rev. Lett. **78**, 4990 (1997).
13. Z. Zhang, X. Sun, M.S. Dresselhaus, J.Y. Ying, J.P. Heremans, Appl. Phys. Lett. **73**, 1589 (1998).
14. J. Heremans, C.M. Thrush, Z. Zhang, X. Sun, M.S. Dresselhaus, J.Y. Ying, D.T. Morelli, Phys. Rev. B **58**, 10091 (1998).
15. M.G. Betti, V. Corradini, U. del Pennino, V. de Renzi, P. Fantini, C. Mariani, Phys. Rev. B **58**, 4231 (1998).
16. F.Y. Yang, K. Liu, D.H. Reich, P.C. Searson, C.L. Chien, Science **284**, 1335 (1999).
17. L. Gavioli, M.G. Betti, C. Mariani, Surf. Sci. **409**, 207 (1998).
18. K. Miki, D.R. Bowler, J.H.G. Owen, G.A.D. Briggs, K. Sakamoto, Phys. Rev. B **59**, 14868 (1999).
19. J.C. Patrin, Y.Z. Li, M. Chander, J.H. Weaver, Phys. Rev. B **46**, 10221 (1992).
20. Y.F. Komnik, E.I. Bukhshtab, Y.V. Nikitin, V.V. Andrievskiĭ, Sov. Phys. JETP **33**, 364 (1971).
21. B. Weitzel, H. Micklitz, Phys. Rev. Lett. **66**, 385 (1991).
22. G. Jezequel, Y. Petroff, R. Pinchaux, F. Yndurain, Phys. Rev. B **33**, 4352 (1986).
23. F. Patthey, W.-D. Schneider, H. Micklitz, Phys. Rev. B **49**, 11293 (1994).
24. A. Tanaka, M. Hatano, K. Takahashi, H. Sasaki, S. Suzuki, S. Sato, Phys. Rev. B **59**, 1786 (1999).
25. J. Thomas, G. Jezequel, I. Pollini, J. Phys. Cond. Mat. **11**, 9571 (1999).
26. R.M. Goodman, G.A. Somorjai, J. Chem. Phys. **52**, 6325 (1970).
27. G. Jezequel, A. Barski, P. Steiner, F. Solal, P. Roubin, R. Pinchaux, Y. Petroff, Phys. Rev. B **30**, 4833 (1984).
28. F. Jona, Surf. Sci. **8**, 57 (1967).
29. L.M. Falicov, P.J. Lin, Phys. Rev. **141**, 562 (1966).
30. M.P. Vecchi, M.S. Dresselhaus, Phys. Rev. B **9**, 3257 (1974).
31. R.A. Herrod, C.A. Cage, R.G. Goodrich, Phys. Rev. B **4**, 1033 (1971).
32. V. Anishchik, L.M. Falicov, F. Yndurain, Surf. Sci. **57**, 375 (1976).